Time-reversal symmetry and covariant Lyapunov vectors for simple particle models in and out of thermal equilibrium

Hadrien Bosetti,* Harald A. Posch,† and Christoph Dellago‡
Computational Physics Group, Faculty of Physics,
University of Vienna, Boltzmanngasse 5, A-1090 Wien, Austria

William G. Hoover§
Ruby Valley Research Institute, Highway Contract 60, Box 598, Ruby Valley 89833, NV USA
(Dated: January 16, 2014)

Recently, a new algorithm for the computation of covariant Lyapunov vectors and of corresponding local Lyapunov exponents has become available. Here we study the properties of these still unfamiliar quantities for a number of simple models, including an harmonic oscillator coupled to a thermal gradient with a two-stage thermostat, which leaves the system ergodic and fully time reversible. We explicitly demonstrate how time-reversal invariance affects the perturbation vectors in tangent space and the associated local Lyapunov exponents. We also find that the local covariant exponents vary discontinuously along directions transverse to the phase flow.

I. INTRODUCTION

Recently, many concepts and methods of dynamical systems theory have turned out to be very useful for the characterization and understanding of physical systems in and out of thermodynamic equilibrium. For example, for a class of stationary nonequilibrium systems, the spectrum of Lyapunov exponents is a convenient tool for studying the collapse of the phase-space probability distribution onto fractal measures with an information dimension smaller than the dimension of phase space. In this case, stationarity is achieved with time-reversible thermostats [1, 2]. Stationary nonequilibrium systems with stochastic thermostats may be formulated along similar lines [3].

The aim of this paper is to apply the hitherto rather unfamiliar concept of covariant Lyapunov vectors and their associated local Lyapunov exponents to some simple and pedagogical systems in equilibrium and in non-equilibrium stationary states to sharpen the intuition for more demanding applications. The systems studied include a harmonic oscillator subjected to a two-stage chain of Nosé-Hoover-type thermostats with a temperature which varies with the position of the particle.

The paper is organized as follows: In the next section we provide the basic theoretical concepts and definitions required for our numerical work. In particular, the covariant vectors and their classical counterparts, the Gram-Schmidt vectors, are introduced, and their dynamical evolution is discussed. Section III is devoted to an alternative differential-equation based method for the evolution of orthonormal perturbation vectors, which may be interpreted as continuous re-orthonormalization. In Sec-

tion IV we specify the protocol for our numerical work, both forward and backward in time. Our main example, a doubly-thermostated oscillator in a space-dependent thermal field, is treated in various subsections of Section V. Section VI is devoted to symplectic systems, with regular trajectories on a torus or with chaotic behavior, for which the differences of the symmetry properties for the local Gram-Schmidt and covariant Lyapunov exponents are most pronounced. We conclude in Section VII with some remarks, which also concern the stationary fluctuation theorem for thermostated systems.

II. COVARIANT LYAPUNOV VECTORS AND LOCAL LYAPUNOV EXPONENTS

If $\mathbf{\Gamma}(t)$ denotes the state of a dynamical system of dimension D, its evolution equations are given by

$$\dot{\mathbf{\Gamma}} = \mathbf{F}(\mathbf{\Gamma}), \qquad (1)$$

where $\boldsymbol{F}$ is a (generally nonlinear) vector-valued function of dimension D. An arbitrary perturbation vector $\delta\mathbf{\Gamma}(t)$ in tangent space evolves according to the linearized equations

$$\dot{\delta\mathbf{\Gamma}} = \mathcal{J}(\mathbf{\Gamma})\delta\mathbf{\Gamma}, \qquad (2)$$

where the dynamical (Jacobian) matrix $\mathcal{J}$ is given by

$$\mathcal{J}(\mathbf{\Gamma}) = \frac{\partial \boldsymbol{F}}{\partial \mathbf{\Gamma}}.$$

The stability of a trajectory in a D-dimensional phase space is determined by a set of D (global) Lyapunov exponents, which are the *time-averaged* logarithmic rates of the growth or decay of the norm of some perturbation vectors, which must be oriented 'properly' in tangent space at the initial time. Formally, let $\mathbf{\Gamma}(0)$ denote the state of the system at time 0, the state at time t is given by $\mathbf{\Gamma}(t) = \phi^t(\mathbf{\Gamma}(0))$, where the map $\phi^t : \mathbf{\Gamma} \to \mathbf{\Gamma}$

*Electronic address: Hadrien.Bosetti@univie.ac.at
†Electronic address: Harald.Posch@univie.ac.at
‡Electronic address: Christoph.Dellago@univie.ac.at
§Electronic address: hooverwilliam@yahoo.com

defines the flow in the phase space $\mathbf{\Gamma}$. Similarly, if $\delta\mathbf{\Gamma}(0)$ is a vector in the tangent space at the phase point $\mathbf{\Gamma}(0)$, at time t, it becomes $\delta\mathbf{\Gamma}(t) = D\phi^t|_{\mathbf{\Gamma}(0)} \, \delta\mathbf{\Gamma}(0)$, where $D\phi^t$ defines the tangent flow. It is represented by a real but generally nonsymmetric $D \times D$ matrix. The multiplicative ergodic theorem of Oseledec [4–6] asserts that there exist 'properly oriented' and normalized vectors $\boldsymbol{v}^\ell(\mathbf{\Gamma}(0))$ in tangent space at $t = 0$, which evolve according to

$$D\phi^t|_{\mathbf{\Gamma}(0)} \, \boldsymbol{v}^\ell(\mathbf{\Gamma}(0)) = \boldsymbol{v}^\ell(\mathbf{\Gamma}(t)), \qquad (3)$$

and which generate the Lyapunov exponents on the way,

$$\pm \lambda_\ell = \lim_{t \to \pm\infty} \frac{1}{|t|} \ln \left\| D\phi^t|_{\mathbf{\Gamma}(0)} \, \boldsymbol{v}^\ell(\mathbf{\Gamma}(0)) \right\| \qquad (4)$$

for all $\ell \in \{1, \ldots, D\}$, both forward and backward in time (for time-reversible systems). (Strictly speaking, this formulation is only correct for nondegenerate exponents λ_ℓ. If two such exponents become identical, the respective vectors must be replaced by a covariant subspace spanned by the vectors. Since in our applications below, this happens only for the symplectic systems in thermodynamic equilibrium discussed in Sec. VI, there is no danger of misinterpretation, and we avoid the additional notational complexity. The case of degenerate exponents is treated in detail in Ref. [7]). Because of the property described by Eq. (3), the vectors $\boldsymbol{v}^\ell$ are called *covariant*. Loosely speaking, covariant vectors are co-moving (co-rotating in particular) with the tangent flow. As will be shown below, this property of co-rotation is responsible for the fact that the evolution of their length in the forward and backward directions of time (for time-reversible systems) is intimately connected, a symmetry not enjoyed by other perturbation vectors. For numerical reasons, it is still necessary to *normalize* the vectors periodically at times $t_n \equiv n\tau$, such that Eq. (4) becomes

$$\lambda_\ell = \lim_{N \to \infty} \frac{1}{N\tau} \sum_{n=0}^{N-1} \ln \left\| D\phi^\tau|_{\mathbf{\Gamma}_n} \, \boldsymbol{v}^\ell(\mathbf{\Gamma}_n) \right\|, \qquad (5)$$

where we use the abbreviated notation $\mathbf{\Gamma}(t_n) \equiv \mathbf{\Gamma}_n$. $\|\boldsymbol{v}^\ell(\mathbf{\Gamma}_n)\| = 1$ at the beginning of each interval of length τ. Generally its norm differs from unity at the end of the interval.

Up to very recently, no practical algorithm for the computation of the covariant vectors was available. The classical algorithm for the computation of Lyapunov exponents [8, 9] is based on the fact that almost all volume elements of dimension $d \leq D$ in tangent space (with the exception of elements of measure zero) asymptotically evolve with an exponential rate, which is equal to the sum of the first d Lyapunov exponents. Such a d-dimensional subspace may be spanned by d orthonormal vectors, which are constructed by the Gram-Schmidt re-orthonormalization procedure and, therefore, are referred to as Gram-Schmidt (GS) vectors $\boldsymbol{g}^\ell(\mathbf{\Gamma}(t))$. The evolution during the time interval $\tau = t_n - t_{n-1}$,

$$D\phi^\tau|_{\mathbf{\Gamma}_{n-1}} \, \boldsymbol{g}^\ell(\mathbf{\Gamma}_{n-1}) \equiv \bar{\boldsymbol{g}}^\ell(\mathbf{\Gamma}_n), \qquad (6)$$

generates a set of non-orthonormal vectors , $\{\bar{\boldsymbol{g}}^\ell(\mathbf{\Gamma}_n), \ \ell = 1, \cdots, D\}$, which after Gram-Schmidt re-orthonormalization [10, 11],

$$\boldsymbol{g}^1(\mathbf{\Gamma}_n) = \frac{\bar{\boldsymbol{g}}^1(\mathbf{\Gamma}_n)}{\|\bar{\boldsymbol{g}}^1(\mathbf{\Gamma}_n)\|},$$

$$\boldsymbol{g}^\ell(\mathbf{\Gamma}_n) = \frac{\bar{\boldsymbol{g}}^\ell(\mathbf{\Gamma}_n) - \sum_{k=1}^{\ell-1} \left(\bar{\boldsymbol{g}}^\ell(\mathbf{\Gamma}_n) \cdot \boldsymbol{g}^k(\mathbf{\Gamma}_n)\right) \boldsymbol{g}^k(\mathbf{\Gamma}_n)}{\left\|\bar{\boldsymbol{g}}^\ell(\mathbf{\Gamma}_n) - \sum_{k=1}^{\ell-1} \left(\bar{\boldsymbol{g}}^\ell(\mathbf{\Gamma}_n) \cdot \boldsymbol{g}^k(\mathbf{\Gamma}_n)\right) \boldsymbol{g}^k(\mathbf{\Gamma}_n)\right\|},$$

(where ℓ consecutively assumes the values $1, \cdots, D$) become the orthonormal starting vectors for the next interval. The vectors $\boldsymbol{g}^\ell$ are not covariant, which means that, in general, the vectors are not mapped by the linearized dynamics into the GS vectors at the forward images of the initial phase-space point [12]. As a consequence, they are also not invariant with respect to the time-reversed dynamics. The Lyapunov exponents are computed from the normalization factors,

$$\lambda_1 = \lim_{N \to \infty} \frac{1}{N\tau} \sum_{n=0}^{N-1} \ln \left\| \bar{\boldsymbol{g}}^1(\mathbf{\Gamma}_n) \right\|,$$

$$\lambda_\ell = \lim_{N \to \infty} \frac{1}{N\tau} \sum_{n=0}^{N-1} \ln \left\| \bar{\boldsymbol{g}}^\ell(\mathbf{\Gamma}_n) \right.$$

$$\left. - \sum_{k=1}^{\ell-1} \left(\bar{\boldsymbol{g}}^\ell(\mathbf{\Gamma}_n) \cdot \boldsymbol{g}^k(\mathbf{\Gamma}_n)\right) \boldsymbol{g}^k(\mathbf{\Gamma}_n) \right\| \qquad (7)$$

for $\ell = 2, \cdots, D$.

Recently, a reasonably fast algorithm for the computation of covariant Lyapunov vectors was presented by Ginelli *et al.* [12], which first requires the construction of the Gram-Schmidt vectors by a forward integration in time. In a second step, this stored information is used to obtain the covariant vectors by a backward iteration in time. For details of this algorithm we refer to their paper [12] and to our previous work [7].

A *local* Lyapunov exponent characterizes the expansion, or shrinkage, of a particular tangent vector during a (short) time interval τ. From Eqs. (5) and (7) local exponents for the covariant and Gram-Schmidt vectors are obtained for a time $t_n \equiv n\tau$ at the phase point $\mathbf{\Gamma}_n$:

$$\Lambda_\ell^{\text{cov}}(t_n) = \frac{1}{\tau} \ln \left\| D\phi^\tau|_{\mathbf{\Gamma}_{n-1}} \, \boldsymbol{v}^\ell(\mathbf{\Gamma}_{n-1}) \right\|, \qquad (8)$$

for $\ell = 1, \cdots, D$, and

$$\Lambda_1^{\text{GS}}(t_n) = \frac{1}{\tau} \ln \left\| \bar{\boldsymbol{g}}^1(\mathbf{\Gamma}_n) \right\|,$$

$$\Lambda_\ell^{\text{GS}}(t_n) = \frac{1}{\tau} \ln \left\| \bar{\boldsymbol{g}}^\ell(\mathbf{\Gamma}_n) \right.$$

$$\left. - \sum_{k=1}^{\ell-1} \left(\bar{\boldsymbol{g}}^\ell(\mathbf{\Gamma}_n) \cdot \boldsymbol{g}^k(\mathbf{\Gamma}_n)\right) \boldsymbol{g}^k(\mathbf{\Gamma}_n) \right\|, \quad (9)$$

for $\ell = 2, \cdots, D$.

Since the spaces

$$\boldsymbol{v}^1 \oplus \cdots \oplus \boldsymbol{v}^\ell = \boldsymbol{g}^1 \oplus \cdots \oplus \boldsymbol{g}^\ell \qquad (10)$$

are covariant subspaces of the tangent space for all ℓ, we have $\boldsymbol{v}^\ell(t) \in \boldsymbol{g}^1(t) \oplus \cdots \oplus \boldsymbol{g}^\ell(t)$. If $\beta_{\ell\ell}(t)$ denotes the angle between the respective covariant and Gram-Schmidt vectors $\boldsymbol{v}^\ell(t)$ and $\boldsymbol{g}^\ell(t)$ at the specified time, the component of the normalized vector $\boldsymbol{v}^\ell(t_{n-1})$ in the direction of $\boldsymbol{g}^\ell(t_{n-1})$ is given by $\cos \beta_{\ell\ell}(t_{n-1})$. During τ, this vector component grows by a factor $\exp\{\Lambda_\ell^{\mathrm{GS}}\tau\}$, whereas the norm of the vector itself grows by $\exp\{\Lambda_\ell^{\mathrm{cov}}\tau\}$. At the end of the interval, equating the vector components of $\boldsymbol{v}^\ell(t_n)$ in the *new* direction of the re-orthonormalized vector $\boldsymbol{g}^\ell(t_n)$, one obtains

$$\Lambda_\ell^{\mathrm{GS}}(t_n) = \Lambda_\ell^{\mathrm{cov}}(t_n) + \frac{1}{\tau} \ln \frac{\cos \beta_{\ell\ell}(t_n)}{\cos \beta_{\ell\ell}(t_{n-1})}, \qquad (11)$$

$\ell = 1, \cdots, D$. This relates the local exponents for the GS and covariant vectors.

If we consider the limit $\tau \to 0$ implying continuous re-orthonormalization of the $\boldsymbol{g}^\ell$ and normalization of the $\boldsymbol{v}^\ell$, Eq. (11) becomes

$$\Lambda_\ell^{\mathrm{GS}}(t) = \Lambda_\ell^{\mathrm{cov}}(t) - \tan \beta_{\ell\ell}(t) \frac{d\beta_{\ell\ell}}{dt}.$$

This is most easily achieved with a matrix of Lagrange multipliers constraining the vectors to unit length and enforcing orthogonality of the $\boldsymbol{g}^\ell$ [13–15]. We shall return to this point in the following section.

For time-continuous systems, these relations are general and are not restricted to any particular model. Below they will be applied to a variety of models mentioned in the introduction.

The global exponents are the time averages of the local exponents over a long trajectory tracing out the whole ergodic phase space component, and are the same for the covariant and Gram-Schmidt cases,

$$\lambda_\ell = \lim_{N \to \infty} \frac{1}{N} \sum_{n=0}^{N-1} \Lambda_\ell^{\mathrm{cov}}(t_n) = \lim_{N \to \infty} \frac{1}{N} \sum_{n=0}^{N-1} \Lambda_\ell^{\mathrm{GS}}(t_n).$$

Whereas the global Lyapunov exponents do not depend on the particular metric and the choice of the coordinate system, the local exponents do. This will become apparent in Section VI for a scaled harmonic oscillator. For particular applications of the local exponents this must be kept in mind.

All systems we consider here are invariant with respect to time reversal. This property leaves the equations of motion in phase and tangent space unchanged if the signs of all momentum-like variables *and* of time are reversed, but leaving all position variables unchanged. This implies that there exists a smooth isometry I of phase space, such that $I\phi^t = \phi^{-t}I$. In practice, an integration of the equations of motion backward in time is carried out with reversed momentum-like variables and a positive time step. After reaching the endpoint, the signs of all momentum-like variables need to be reversed again and the time variable properly adjusted. Alternatively, and even more easily, the integration of the motion

equations may proceed without changing the sign of the momentum-like variables but with a negative time step. There is also no sign change after reaching the end point in this case. A comparison of both methods yields identical results. Where necessary, we indicate the forward and backward directions of time by upper indexes $(+)$ and $(-)$, respectively. If this index is omitted, the forward direction is implied.

We have mentioned already that the classical algorithm invoking Gram-Schmidt re-orthonormalization carefully keeps track of the time evolution of d-dimensional volume elements, $\delta\mathcal{V}_d$, for any $d \leq D$, which proceeds according to [2, 16]

$$\frac{d \ln \delta\mathcal{V}_d(t)}{dt} = \sum_{\ell=1}^{d} \Lambda_\ell^{\mathrm{GS}}(t).$$

If the total phase volume is conserved as for symplectic systems, the following sum rule for the Gram-Schmidt local exponents holds at all times:

$$\sum_{\ell=1}^{D} \Lambda_\ell^{\mathrm{GS}}(t) = 0. \qquad (12)$$

In this symplectic case we can even say more. For each positive local GS exponent there is a local negative GS exponent such that their pair sum vanishes [17],

$$^{(+)}\Lambda_\ell^{\mathrm{GS}}(t) = -^{(+)}\Lambda_{D+1-\ell}^{\mathrm{GS}}(t), \qquad (13)$$

$$^{(-)}\Lambda_\ell^{\mathrm{GS}}(t) = -^{(-)}\Lambda_{D+1-\ell}^{\mathrm{GS}}(t). \qquad (14)$$

As indicated, such a symplectic local pairing symmetry exists both forward and backward in time. But, generally, the GS local exponents do not show the symmetry with respect to time-reversal invariance. Thus,

$$^{(-)}\Lambda_\ell^{\mathrm{GS}}(t) \neq -^{(+)}\Lambda_{D+1-\ell}^{\mathrm{GS}}(t). \qquad (15)$$

No such symmetries exist for non-symplectic systems. Examples are provided below.

The situation is very different for the covariant local Lyapunov exponents. In their case, the vectors are still re-normalized, but the angles between them remain unchanged, which effectively destroys all information concerning the d-dimensional volume elements. Thus, no symmetries analogous to Eqs. (13) and (14) exist. Instead, the re-normalized covariant vectors faithfully preserve the time-reversal symmetry of the equations of motion, which is reflected by

$$^{(-)}\Lambda_\ell^{\mathrm{cov}}(t) = -^{(+)}\Lambda_{D+1-\ell}^{\mathrm{cov}}(t) \text{ for } \ell = 1, \cdots, D, \qquad (16)$$

regardless, whether the system is symplectic or not. This means that an expanding co-moving direction is converted into a collapsing co-moving direction by an application of the time-reversal operation. Of course, the

forward and backward local exponents in Eq. 16) refer to the same phase space point $\mathbf{\Gamma}(t)$.

These symmetry properties may be considered the main conceptual differences between the Gram-Schmidt and covariant viewpoints.

Before leaving this section, a short remark concerning the commonly-used term "time-dependent exponent" seems in order. Primarily, this quantity is a function of the phase point and should only be called a "local" exponent. Its value may be different whether the phase point is reached from the past, forward in time $(+)$, or from the future, backward in time $(-)$.

III. DIFFERENTIAL APPROACH TO LOCAL LYAPUNOV EXPONENTS

Equation (9) precisely reflects the numerical procedure for the computation of local GS exponents for finite time intervals τ. But it is also possible to obtain a differential version for $\tau \to 0$. Goldhirsch *et al.* derived a full set of differential equations for the Gram-Schmidt vectors $\mathbf{g}^\ell$ [13],

$$\dot{\mathbf{g}}^1 = \mathcal{J}\mathbf{g}^1 - R_{11}\,\mathbf{g}^1, \tag{17}$$

$$\dot{\mathbf{g}}^\ell = \mathcal{J}\mathbf{g}^\ell - R_{\ell\ell}\,\mathbf{g}^\ell - \sum_{m=1}^{\ell-1}(R_{\ell m} + R_{m\ell})\,\mathbf{g}^m, \tag{18}$$

where in the last equation $\ell = 2, \cdots, D$. We have demonstrated [14, 15] that the matrix elements

$$R_{\ell m}(\mathbf{\Gamma}(t)) = (\mathbf{g}^\ell)^T \mathcal{J}\mathbf{g}^m \tag{19}$$

may be understood as Lagrange multipliers enforcing the orthonormalization constraints $\mathbf{g}^\ell \cdot \mathbf{g}^m = \delta_{\ell m}$ (equal to unity for $\ell = m$, and zero otherwise). Here T means transposition. Most importantly, the diagonal elements are the local Gram-Schmidt exponents:

$$\Lambda_\ell^{\mathrm{GS}}(\mathbf{\Gamma}(t)) \equiv R_{\ell\ell}(\mathbf{\Gamma}(t)) = (\mathbf{g}^\ell)^T \mathcal{J}\mathbf{g}^\ell. \tag{20}$$

This expression nicely underlines the local nature of the exponents.

We have verified for the doubly-thermostated heat conduction model discussed in Sec. V below that the direct integration of the Eqs. (17,18) provide local GS exponents according to Eq. (20), which agree extremely well with the results obtained from a direct application of the GS algorithm, Eq. (9), for a reasonably-small time interval τ. This agreement also persists for the time-reversed dynamics.

IV. NUMERICAL CONSIDERATIONS

In this section we remark on a few aspects of our implementation of the algorithm for the computation of the covariant Lyapunov vectors, which we apply in the following sections. Reduced units are used for the various models treated below. For convenience, we specify already here the adopted values (in reduced units) for some time parameters: $t_\omega = 6 \times 10^4$, $t_\alpha = 5 \times 10^4$, and $t_0 = 100$. Their meaning is explained below. For the integration of the equations of motion, a 4th-order Runge-Kutta algorithm with a time step $dt = 0.001$ is used. This time step is chosen such that the trajectory is correct to double-precision accuracy. For the interval between successive Gram-Schmidt re-orthonormalization steps – respective covariant vector normalizations – we choose $\tau = 10dt = 0.01$. This number is a (very conservative) compromise between the achieved reduction in storage requirements as outlined below, and the precision of integration forward and backward over the same interval. The time t_0 is chosen such that in the interval $-t_0 \le t \le t_0$ accurate Gram-Schmidt and covariant Lyapunov vectors are available.

The simulations are carried out with the following protocol:

Phase 1 (forward integration from $-t_\omega$ to $+t_\omega$): Starting with arbitrary initial conditions at a time $-t_\omega$ and using a positive integration time step $dt > 0$, the evolution of the reference trajectory $\mathbf{\Gamma}(t)$ and of the full set of Gram-Schmidt vectors is computed in the forward direction of time up to a time $+t_\omega$. The reference trajectory and the Gram-Schmidt vectors are stored for every 10 time steps, $10dt = \tau$, along the way. The Gram-Schmidt vectors are used in phase 2 for the construction of the covariant vectors, and the reference trajectory is required in phase 3 for the computation of the time-reversed Gram-Schmidt vectors. The Lyapunov spectrum $\{^{(+)}\lambda^{\mathrm{GS}}\}$ is accumulated for times $-t_\alpha \le t \le t_\omega$, for which the orientations of the Gram-Schmidt vectors are fully relaxed.

Phase 2 (backward iteration from t_ω to $-t_0$): Starting at t_ω, the covariant vectors are computed by iterating back to a time $-t_0$. The details of this algorithm are given in Ref. [7]. Since the *forward* GS-vectors, stored during phase 1, are now used in reversed order, the consecutive order of the covariant vectors $\cdots, \mathbf{v}^\ell(t_n), \mathbf{v}^\ell(t_{n-1}), \cdots$ has to be reversed for the computation of the corresponding local exponent,

$$^{(+)}\Lambda_\ell^{\mathrm{cov}}(t_n) = \frac{1}{\tau}\ln\frac{\|\mathbf{v}^\ell(t_n)\|}{\|\mathbf{v}^\ell(t_{n-1})\|},$$

or, alternatively, the sign of the local exponents must be reversed. The time averaging for the global Lyapunov spectrum $\{^{(+)}\lambda_\ell^{\mathrm{cov}}\}$ is carried out for times $t_\alpha \ge t \ge -t_0$.

The following two phases are only required for the computation of the local *time-reversed* Gram-Schmidt and covariant exponents.

Phase 3 (backward integration from t_ω to $-t_\omega$): With arbitrary initial conditions at time t_ω, the Gram-Schmidt tangent space dynamics is followed backward in time up to $-t_\omega$. To counteract the Lyapunov instability, it is essential for this computation to use the *same* reference trajectory stored in phase 1, where the sign of

the momentum-like variables (p, z, and x for the doubly-thermostated oscillator) is left unchanged, but with the time step reversed to -0.001. For an accurate computation of the backward GS vectors, the reference trajectory at *every* integration step is required. Since in phase 1 this information was stored for only every 10th step (to save computer storage), the forward reference trajectory is piece-wise re-computed with stored phase-space points as initial conditions. The backward Gram-Schmidt vectors are again stored for every 10th time step replacing the forward vectors of phase 1. If time is reversed, the stable directions become unstable and *vice versa*. The Lyapunov spectrum $\{^{(-)}\lambda_\ell^{\mathrm{GS}}\}$ is accumulated in the interval $t_\alpha \geq t \geq -t_\omega$.

Phase 4 (forward iteration from $-t_\omega$ to $+t_0$): Analogous to phase 2, in this final stage the covariant Lyapunov vectors for the *reversed time direction* are computed with the help of the time-reversed Gram-Schmidt vectors from phase 3. The respective Lyapunov spectrum $\{^{(-)}\lambda_\ell^{\mathrm{cov}}\}$ is accumulated for times $-t_\alpha \leq t \leq t_0$.

It may be noticed that in the interval $-t_0 \leq t \leq +t_0$ all local properties are available with the Gram-Schmidt and covariant vectors fully relaxed both forward and backward in time. Therefore, the detailed analysis of local (time-dependent) Lyapunov exponents in the following sections is carried out in this regime.

V. DOUBLY-THERMOSTATED OSCILLATOR

A. Description of the model

Here we consider a simple model which already has many ingredients in common with much more involved physical systems. It exhibits chaotic equilibrium and stationary nonequilibrium states and collapses onto a limit cycle for very strong driving. It consists of a one-dimensional harmonic oscillator, which is coupled to two consecutive stages of Nosé-Hoover thermostats with a space-dependent temperature $T(q)$. The equilibrium version of this model was first considered by Martyna, Klein and Tuckerman [18]. Its nonequilibrium properties were consecutively studied by us in some detail [19, 20], but without considering covariant vectors. This paper is also intended to augment this work correspondingly.

The equations of motion, expanded with two thermostat variables z and x, are [19, 20]

$$\begin{aligned}
\dot{q} &= p, \\
\dot{p} &= -q - zp, \\
\dot{z} &= p^2 - T(q) - zx, \\
\dot{x} &= z^2 - T(q),
\end{aligned}$$

where the position dependent temperature is given by

$$T(q) = 1 + \varepsilon \tanh(q).$$

The control parameter ε coincides with the temperature gradient at $q = 0$. These equations are written in the most simple reduced form with all arbitrary parameters of the model set equal to unity. The system is not symplectic. On average, the oscillator picks up energy from the thermostat whenever it is in a region of high temperature ($q > 0$), and releases it again in low-temperature regions ($q < 0$).

B. Global properties

For a typical non-equilibrium state, ($\varepsilon = 0.25$), the global Lyapunov spectrum was computed by four independent methods, applying the protocol outlined in Sec. IV:

Phase 1 : GS exponents in forward direction of time,
$$\{^{(+)}\lambda_\ell^{\mathrm{GS}}\} = \{0.053_1, 0.0000_1, -0.034_4, -0.086_7\},$$

Phase 2 : covariant exponents in forward direction of time
$$\{^{(+)}\lambda_\ell^{\mathrm{cov}}\} = \{0.053_6, 0.0000_1, -0.035_1, -0.086_2\},$$

Phase 3 : GS exponents in backward direction of time
$$\{^{(-)}\lambda_\ell^{\mathrm{GS}}\} = \{0.086_7, 0.034_4, 0.0000_3, -0.053_1\},$$

Phase 4 : covariant exponents in backward direction of time
$$\{^{(-)}\lambda_\ell^{\mathrm{cov}}\} = \{0.087_1, 0.033_7, 0.00000_1, -0.052_5\}.$$

The last digit of each number is rounded accordingly. Considering the smallness of the exponents and the rather involved numerical procedures, the agreement between the independently-determined global spectra is very satisfactory. A comparison of the forward and backward dynamics reveals the theoretically expected symmetry for the global Lyapunov exponents [5, 21],

$$^{(-)}\lambda_\ell = -^{(+)}\lambda_{D+1-\ell} \text{ for } \ell = 1, \cdots, D. \quad (21)$$

If the temperature gradient ε is varied over a wide range, significant changes of the spectrum become evident. This is shown in the top panel of Fig. 1. There exist a number of distinct regimes with different qualitative behavior.

For $\varepsilon \lesssim 0.18$, the spectrum changes but little with ε, and the Kaplan-Yorke dimension is only weakly reduced with respect to the full phase space dimension, as is shown in the bottom panel of Fig. 1. The dissipation due to the weak heat current influences the appearance of the chaotic phase-space trajectory very little. An example of a projection of such a trajectory onto the qpz-subspace is provided in the top panel of Fig. 5.

For $0.18 \lesssim \varepsilon < 0.26$, the trajectory is more and more attracted to a weakly unstable periodic orbit (see the
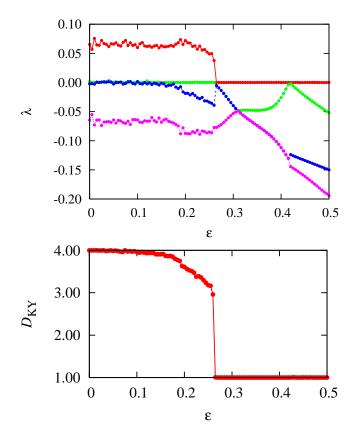
FIG. 1: (Color online) Temperature-gradient dependence of all four Lyapunov exponents (top panel) and of the Kaplan-Yorke dimension (bottom panel) for the doubly-thermostated oscillator. For $\varepsilon > \varepsilon_c = 0.26314$, the trajectory collapses onto a limit cycle.

FIG. 2: (Color online) Floquet multipliers μ_2 and μ_3 in the complex plain for $\varepsilon \geq 0.26312$. UC denotes the unit circle, and A is the bifurcation point. The multipliers are complex conjugate to each other for $\varepsilon > 0.26319$ as indicated by B.

C. Local Lyapunov exponents

In Fig. 5 we apply Eq. (11) to the doubly-thermostated oscillator in a stationary chaotic state, $\varepsilon = 0.25$. For $\ell = 1$ the respective time-dependent exponents are identical and are not shown. The case $\ell = 2$ is treated in the figure. The dashed green line denotes the covariant local exponent, the smooth red line is for the local GS-exponents, which is directly obtained from the simulation invoking Gram-Schmidt re-orthonormalization. The time interval τ is 0.01. The blue points for $\Lambda_\ell^{\mathrm{GS}}(t)$ are computed with Eq. (11), where the covariant exponent $\Lambda_\ell^{\mathrm{COV}}(t)$ and the angle $\beta_{\ell\ell}(t)$ are taken from the simulation. The agreement is convincing. Similar results are also obtained for $\ell = 3$ and 4 (not shown).

In the bottom panel of Fig. 6 we demonstrate, for $\ell = 2$, the general time-reversal symmetry for the local (time dependent) covariant exponents (see Eq. (16) which also gives rise to the symmetry of the global (time-averaged) exponents already encountered in Eq. (21). For $\ell = 1$ the symmetry is also fully obeyed but not shown.

As emphasized already in Eq. (15), the local Gram-Schmidt exponents generally do not have this symmetry. This is explicitly shown in the top panel of Fig. 6. See also Ref. [20], where the same observation was made. Only the subspaces in Eq. (10) spanned by consecutive Gram-Schmidt vectors have a simple dynamical interpretation, but not the GS-vectors themselves. The orthonormal GS-vectors are oriented such that for the tangent space, tangent to the phase flow at the phase point $\boldsymbol{\Gamma}(t)$, the subspaces $^{(-)}\boldsymbol{g}^1(t) \oplus \cdots \oplus ^{(-)}\boldsymbol{g}^\ell$, with $\ell \in \{1, \cdots, D\}$, are the most unstable subspaces of dimension ℓ going from time t to $-\infty$ (i.e. the most stable subspaces of dimension ℓ in the future). Although time reversal converts a most stable subspace of dimension ℓ into the most unstable subspace with the same dimen-

bottom panel of Fig. 5), which for $\varepsilon_c \approx 0.26312$ turns into a stable limit cycle as shown in the top panel of Fig. 4. The nature of this transition may be established by considering the Floquet multipliers μ_ℓ, $\ell = 1, \cdots, 4$ for the fixed points of the Poincaré map, defined by $q = 0$, for $\varepsilon \geq \varepsilon_c \approx 0.26312$. Whereas $\mu_1 = 1$ and $\mu_4 < 0$, a single mutiplier μ_2 crosses the unit circle on the real axis at the point A corresponding to ε_c in Figure 2. Such a behavior is characteristic of a period doubling bifurcation [22], where, possibly, the chaotic attractor disappears in a boundary crisis bifurcation. This point will be studied separately [23]. Increasing ε further, the Floquet multipliers $\mu_{2,3}$ vary as indicated by the arrows and become complex conjugate to each other for $\varepsilon \approx 0.26319$ (point B in Fig. 2).

For $\varepsilon \approx 0.417$, there is another transition changing the two-loop limit cycle into a single-loop orbit. This is illustrated in the bottom panel of Fig. 4 and will be studied separately [23].
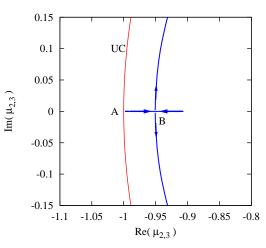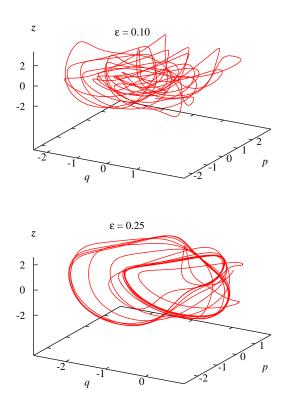
FIG. 3: (Color online) Projection of a short chaotic trajectory for $\varepsilon = 0.10$ (top) and $\varepsilon = 0.25$ (bottom) onto the qpz-subspace.

FIG. 4: (Color online) Projection of the limit cycle for $\varepsilon = 0.28$ (top) and $\varepsilon = 0.45$ (bottom) onto the qpz-subspace.

sion, and *vice versa*, there is no obvious correlation of the instantaneous Lyapunov exponents $^{(-)}\Lambda_\ell^{\mathrm{GS}}(t)$ and $^{(+)}\Lambda_{D+1-\ell}^{\mathrm{GS}}(t)$ for $\ell = 1, \cdots, D$.

It is interesting to follow the time dependence of the covariant local exponents, or more correctly expressed, their variation for consecutive state points along the phase space trajectory (see Fig. 7). One observes that the order of the exponents fluctuates and may even be totally reversed with $\Lambda_1^{\mathrm{cov}}(t)$ being most negative and $\Lambda_4^{\mathrm{cov}}(t)$ most positive. Also the dimension of the stable and unstable manifolds changes along the trajectory. This indicates that the system is far from being hyperbolic. We address this point more closely in the following subsection.

D. Hyperbolicity

We infer from Eq. (11) that the difference between the local covariant and Gram-Schmidt exponents stems from the fact that the angle between the respective vectors deviates significantly from zero and varies with time. But also the angles between covariant vectors, $\alpha_{ij}(t) \equiv \arccos[(\boldsymbol{v}^i \cdot \boldsymbol{v}^j)/|\boldsymbol{v}^i||\boldsymbol{v}^j|]$ significantly change with time.
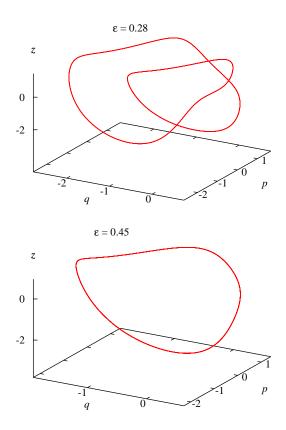
This is demonstrated in the bottom panel of Fig. 8 for the same nonequilibrium state ($\varepsilon = 0.25$) of the doubly-thermostated oscillator discussed previously. There is an intermittent tendency of any two pairs of vectors to get parallel or antiparallel to each other. The probability distributions for these angles, $\pi(\alpha_{ij})$, are shown in the top panel of Fig. 8 and confirm this observation. Although the angles α do not become strictly zero – the vectors could not separate anymore after such an event, which is not observed – the large probability for angles close to zero or π is noticeable. As was mentioned before, the associated local covariant exponents are out of order for most of the time as in Fig. 7. If P_i denotes the probability for Λ_i^{cov} to be out of order with respect to any of the other exponents, one finds for the doubly-thermostated oscillator ($\varepsilon = 0.25$) $\{P_1, \cdots, P_4\} = \{0.650, 0.813, 0.840, 0.645\}$. This clearly demonstrates the strong entanglement between the covariant vectors. If the local exponents are time averaged along the trajectory for time intervals Δ, the analogous probabilities $\overline{P}_i^\Delta$ for the time-averaged exponents $\overline{\Lambda_i^{\mathrm{cov}}}^\Delta$ scale according to $\overline{P}^\Delta \propto \Delta^{-\gamma_i}$ with $\gamma > 0$ for large-enough Δ. This shows that the domination of the Oseledec splitting is violated for finite times.
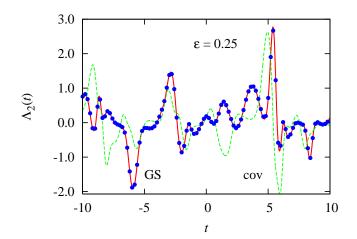
Such a behavior is in contrast to the covariant dynam-

FIG. 5: (Color online) Time-dependence of the local Lyapunov exponents $\Lambda_2(t)$ in the forward direction of time for the doubly-thermostated oscillator with $\epsilon = 0.25$. The smooth red curve denotes Gram-Schmidt exponents, directly obtained with a re-orthonormalization procedure, the blue points are computed with Eq. (11), using the covariant time-dependent exponents $\Lambda_\ell^{\text{cov}}$ (also shown as green dashed line) and the angles $\beta_{\ell\ell}$ as input. For clarity, only every 20th point is depicted.

ics of hard-disk systems, for which the covariant vectors tend to avoid becoming parallel or antiparallel [7]. Thus, whereas the hard-disk system is hyperbolic, the doubly-thermostated oscillator is not.

E. Singularities of the local Lyapunov exponents

In the direction of the flow, the local Lyapunov exponents clearly are smooth functions of the time and, hence, of the phase-space position along the trajectory, see Fig. 5. But transverse to the flow this need not be the case. Indeed, for the periodic Lorentz gas it was noted by Gaspard [24, 25] that the local stretching factors are discontinuous transverse to the flow. Since this model involves hard elastic collisions of point particles with space-fixed scatterers, the observed discontinuity might still be thought to be a consequence of the discontinuous nature of the flow. However, Dellago and Hoover showed [26] that this is not the case. They found a discontinuous local exponent Λ_1^{GS} along a path transverse to the flow even for a time-continuous Hamiltonian system, a chaotic pendulum on a spring. Of course, their result also applies to Λ_1^{cov} for that model. Here we provide evidence for the doubly-thermostated oscillator in equilibrium ($\varepsilon = 0$) that all local covariant exponents are discontinuous along directions transverse to the flow.

For this simulation we slightly modify the protocol of Section IV.

Phase 0: Starting at a phase point $\mathbf{\Gamma}_s$ at time zero, the reference trajectory is followed backward in time to $-t_\omega = -60,000$ and is periodically stored for intervals τ
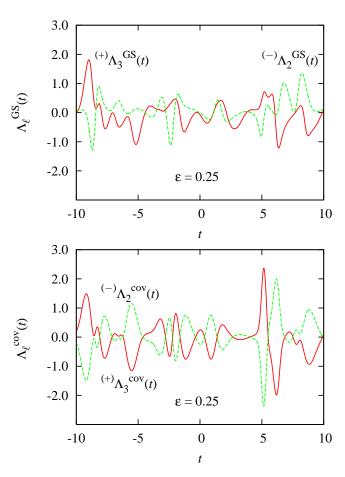

FIG. 6: (Color online) Doubly-thermostated oscillator for $\epsilon = 0.25$. Top panel: The Gram-Schmidt local Lyapunov exponents do not display time-reversal symmetry. Bottom panel: Display of time-reversal symmetry by the covariant local exponents, $^{(+)}\Lambda_\ell^{\text{cov}} = -^{(-)}\Lambda_{D+1-\ell}^{\text{cov}}$ for $\ell = 2$, Analogous curves are obtained for the other ℓ, but are not shown.

along the way.

Phase 1: The next phase is identical to phase 1 of Section IV with one essential difference: For $-t_\omega \leq t \leq 0$, the previously-stored reference trajectory is now used in the forward direction of time for the computation of the Gram-Schmidt vectors, which assures that the trajectory precisely arrives at $\mathbf{\Gamma}_s$ at time zero in spite of the inherent Lyapunov instability. For $0 \leq t \leq t_\omega$ the simulation proceeds as in phase 1 of Section IV.

Phase 2: This is identical to phase 2 of Section IV and provides us with the covariant vectors and the respective local exponents in the interval $-t_0 < t < t_0$ and at the time $t = 0$ in particular, when the state coincides with the selected phase point $\mathbf{\Gamma}_s$.

The whole procedure is repeated for starting points $\mathbf{\Gamma}_s \equiv \mathbf{\Gamma}_0 + s \times (0, 0, 1, 0)$ on a straight line parallel to the z-axis, which is parametrized by s. This line is transversal to the flow, as may be expected from Fig. 5.

As an example, we plot in the top panel of Fig. 9 the local covariant exponent $\Lambda_4^{\text{cov}}(t)$ as a function of time
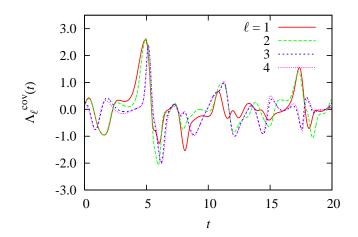
FIG. 7: (Color online) Doubly-thermostated oscillator with $\epsilon = 0.25$: Time dependence of all four local covariant Lyapunov exponents.

for 500 initial points $\mathbf{\Gamma}_s$ separated by $\Delta s = 1 \times 10^{-4}$. It should be noted that the scale on the t axis, converted into distances along the trajectory, is about 200 times coarser than that on the s axis. The red line for $t = 0$ connects the local exponents for the selected initial states $\mathbf{\Gamma}_s$. This curve for $\Lambda_4^{\text{cov}}(t)$ is also reproduced in the bottom panel of Fig. 9 together with an analogous result for $\Lambda_1^{\text{cov}}(t)$. Both curves exhibit singularities on many scales showing singular fractal character. There are no obvious correlations between the two curves. The singularities are due to bifurcations in the past history of the trajectory. In view of Fig. 5, such a bifurcation may be visualized, for example, by a transition of the trajectory from the neighborhood of an unstable periodic orbit to the neighborhood of another with a different number of loops.

One may raise the question (as has been done by one of the referees), how reliable the curves in Fig. 9 are in view of the chaotic nature of the flow and problems of shadowing due to the finite computational accuracy. An increase of the Runge-Kutta integration time step dt by a factor of four has no noticeable effect (less than 0.1%) in Fig. 9, which also proved completely insensitive to a reduction of the relaxation time t_ω of the algorithm by a factor of two and of an increase of the time τ between successive re-orthonormalization steps by the same factor. This robustness, however, does not apply to the local exponents Λ_2^{cov} and Λ_3^{cov} (not shown), which belong to the two-dimensional central manifold for this equilibrium system. The respective covariant vectors span this subspace, but their precise orientations and their local exponents are affected by details of the algorithm and do not have direct physical significance.

For nonequilibrium stationary states the singular character of the local exponents in transverse directions is expected to be even more pronounced, since even the phase-space probability density becomes a multifractal object [1, 14]. For the covariant exponent this cannot
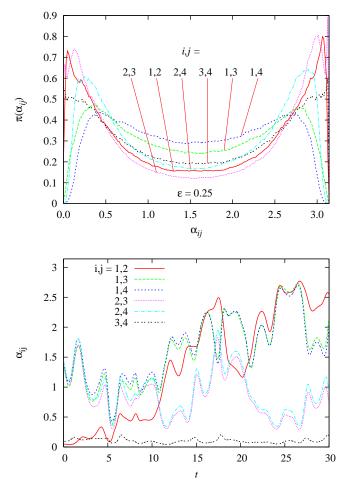

FIG. 8: (Color online) Doubly-thermostated oscillator with $\epsilon = 0.25$. Top panel: Probability distributions for the angles α_{ij} between covariant vector pairs specified by the labels. Bottom panel: Time evolution of the angles α_{ij} between the covariant vectors $\boldsymbol{v}^i$ and $\boldsymbol{v}^j$.

be shown with the present algorithm. The reason is that during the time-reversed simulation in phase 0, the phase volumes collapse yielding negative Lyapunov exponent sums. Since in phase 1 this trajectory is followed in the opposite direction, the respective phase volumes *expand* providing a positive sum of Lyapunov exponents, but only up to time zero. For positive times the reference trajectory is calculated anew from the motion equations, again yielding *contracting* phase volumes. Thus, the character of the flow changes at $t = 0$ and the Gram-Schmidt vectors at first are non-relaxed and point into wrong directions for positive times. Since these vectors are required for the computation of covariant vectors at and near zero time, the algorithm cannot be used to obtain the covariant vectors and respective local exponents at a pre-determined point $\mathbf{\Gamma}_s$ in phase space. For equilibrium states this restriction does not apply and the local exponents may be computed for pre-specified phase-space points.
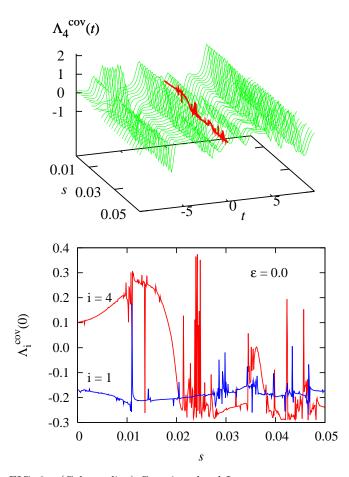
FIG. 9: (Color online) Covariant local Lyapunov exponent, Λ_4^{cov}, for the doubly-thermostated oscillator in equilibrium. Top panel: Time dependence along trajectories, which, for $t = 0$, are at the specified initial points $\mathbf{\Gamma}_s$ introduced in the main text. These phase points lie on a straight line transverse to the flow, and s specifies the precise position. The variation of the local exponent along this straight line is shown as a red curve. Bottom panel: The red curve is a magnified view of the red line of the upper panel, representing the variation of Λ_4^{cov} along a straight line transverse to the flow in the phase space. The blue line is an analogous curve for Λ_1^{cov}.

VI. LOCAL LYAPUNOV EXPONENTS FOR SYMPLECTIC SYSTEMS

So far we have omitted to mention that we use a particular metric in phase space. Whereas the global exponents are independent of the metric, the local exponents, covariant or Gram-Schmidt, clearly are not. We demonstrate this with the most simple symplectic example, a scaled harmonic oscillator [27, 28] with Hamiltonian

$$H_s(p,q) = \frac{1}{2}\left[\left(\frac{p}{s}\right)^2 + (sq)^2\right]$$

and equations of motion

$$\dot{q} = s^{-2}p, \quad \dot{p} = -s^2q, \qquad (22)$$

where s is a scaling parameter. For the 'natural' scaling, $s = 1$, the global and local exponents vanish. But for the
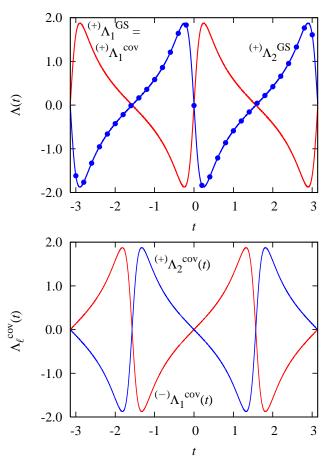

FIG. 10: (Color online) Scaled harmonic oscillator with $s = 2$: Time dependence of the local Lyapunov exponents. Top panel: The smooth red lines are local GS exponents for $\ell = 1$ and 2 as indicated by the labels. The results from direct simulation and from theory are undistinguishable on this scale. The points indicate the reconstruction of $^{(+)}\Lambda_2^{\text{GS}}$ with the help of Eq. (11), where $^{(+)}\Lambda_2^{\text{cov}}$ is shown in the lower panel. Note that the GS and covariant exponents for $\ell = 1$ are identical. Bottom panel: Demonstration of the time-reversal invariance for the covariant exponents.

scaled case, $s \neq 1$, the local Lyapunov exponents do not. They depend on the metric and, for that matter, on the choice of the coordinate system, be it Cartesian or polar.

Let us look at this model in a little more detail, since the dynamical matrix

$$\mathcal{J} = \begin{pmatrix} 0 & s^{-2} \\ -s^2 & 0 \end{pmatrix}$$

for this linear model does not depend on the phase point and allows for a complete analytical solution [28] for the tangent vector dynamics. Still, the model is a bit peculiar, since there is no global exponential ordering of tangent vectors familiar from the Gram-Schmidt algorithm, and the considerations of Sec. IV lose their meaning. Any (unit) vector, with arbitrary initial condition

(phase), which is a solution of Eq. (17), may be taken as the first Gram-Schmidt vector (or covariant vector for that matter). We fix this arbitrary phase by requiring that $\boldsymbol{g}^1$ coincides with the normalized phase-space velocity, which is associated with a vanishing exponent and is a solution of Eq. (17), as may be explicitly shown. Thus,

$$\boldsymbol{g}^1 \equiv \begin{pmatrix} \delta q_1 \\ \delta p_1 \end{pmatrix} = \left[\left(\frac{p}{s^2} \right)^2 + (s^2 q)^2 \right]^{-1/2} \begin{pmatrix} p/s^2 \\ -s^2 q \end{pmatrix}, \quad (23)$$

where we denote the perturbation components of $\boldsymbol{g}^1$ by δq_1 and δp_1). From the constrained motion equation (17) one obtains

$$\dot{\delta q_1} = s^{-2} \delta p_1 - R_{11} \delta q_1 \qquad (24)$$
$$\dot{\delta p_1} = -s^2 \delta q_1 - R_{11} \delta p_1. \qquad (25)$$

Since $\boldsymbol{g}^1$ is constrained to unit length, $\delta q_1 \dot{\delta q_1} + \delta p_1 \dot{\delta p_1} = 0$, and noting that $\Lambda_1^{\mathrm{GS}} \equiv R_{11}$, we obtain from these equations

$$\Lambda_1^{\mathrm{GS}} = \left(s^{-2} - s^2 \right) \delta q_1 \delta p_1. \qquad (26)$$

Insertion of δq_1 and δp_1 from Eq. (23) yields an analytic expression for the local Gram-Schmidt exponent Λ_1^{GS} as a function of the phase-space point (q, p). The second Gram-Schmidt vector is perpendicular to the first, and its associated GS exponents immediately follow from the conservation of phase-space volume:

$$\Lambda_2^{\mathrm{GS}}(q, p) = -\Lambda_1^{\mathrm{GS}}(q, p).$$

In the top panel of Fig. 10 the local Gram-Schmidt exponents for the scaled harmonic oscillator for $s = 2$ are shown as a function of time. The initial conditions $q(0) = 0$ and $p(0) = 1$ are used, for which the solution of Eq. (22) becomes

$$q(t) = s^{-2} \sin t \,, \quad p(t) = \cos t.$$

Both computer simulation results and the theoretical expressions for Λ_1^{GS} and Λ_2^{GS} are shown, which agree so well that they cannot be distinguished and appear only as a single smooth red line in the figure.

The upper and lower bounds of the local exponents are also easily obtained from Eq. (26) [28],

$$\Lambda_{\mathrm{min,max}} = \pm(s^{+2} - s^{-2})/2.$$

The extrema are attained whenever the components δq and δp of the respective perturbation vectors contribute equally, $\delta p = \pm \delta q$. For $s = 2$ we find $\Lambda_{\mathrm{min,max}} = \pm 1.875$ in full agreement with Fig. 10.

The undetermined phases we encountered with the Gram-Schmidt vectors also carry over to the covariant vectors. But since the latter are computed with the help of the former, the choice of phase for $\boldsymbol{g}^1$ also fixes that for

$\boldsymbol{v}^1$ and $\boldsymbol{v}^2$. In the lower panel of Fig. 10 the covariant exponent $\Lambda_2^{\mathrm{cov}}(t)$ is shown as it is obtained from the simulation. If this function is used to reconstruct $\Lambda_2^{\mathrm{GS}}(t)$ with the help of Eq. (11), the (blue) dots in the upper panel of Fig. 10 are obtained, where $\cos(\beta_{22}) = \boldsymbol{g}^2 \cdot \boldsymbol{v}^2$ is also taken from the simulation. The agreement is very good. In the lower panel of Fig. 10 we also plot $^{(-)}\Lambda_1^{\mathrm{cov}}(t)$ for the time-reversed dynamics. The time-reversal symmetry of Eq. (16),

$$^{(-)}\Lambda_1^{\mathrm{cov}}(t) = -^{(+)}\Lambda_2^{\mathrm{cov}}(t),$$

is nicely displayed.

As a slightly more involved example, we compute the four local Lyapunov exponents for the symplectic Hénon-Heiles system [29] with Hamiltonian

$$H = \frac{1}{2}(p_x^2 + p_y^2) + \frac{1}{2}(x^2 + y^2) + x^2 y - \frac{1}{3}y^3. \qquad (27)$$

For an energy $H = 1/6$, the system is known to be chaotic (with a Lyapunov spectrum $\{0.127_7, 0, 0, -0.127_7\}$), where the trajectory visits most of the accessible phase space [30, 31]. Using the protocol of Section IV, we compute the GS and covariant exponents and present some of the results in Fig. 11. In the top panel the symplectic local pairing symmetry of Eq. (13) for $^{(+)}\Lambda_2^{\mathrm{GS}}$ and $^{(+)}\Lambda_3^{\mathrm{GS}}$ is shown by the smooth red lines (similar to the results of Ref. [31]). The green dashed line refers to the time-reversed exponent $^{(-)}\Lambda_3^{\mathrm{GS}}$ and clearly emphasizes the lack of any time-reversal symmetry as expressed by the inequality (15). On the other hand, for the covariant exponents precisely this symmetry is evident from the lower panel of Fig. 11.

To avoid confusion, we note that the 'detailed balance symmetry' introduced in Ref. [31] is not connected with the symplectic local pairing symmetry considered here. The former only means that for a global exponent to become zero, the positive and negative parts of the respective local exponent along the trajectory must cancel each other when integrated over time.
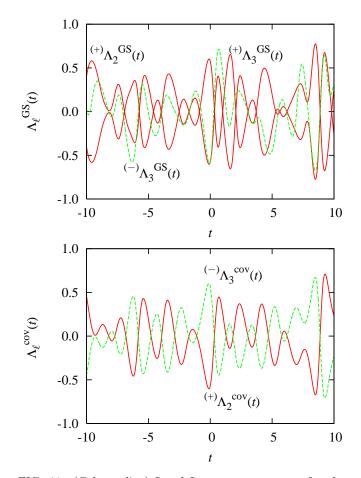
FIG. 11: (Color online) Local Lyapunov exponents for the Hénon-Heiles system with energy $H = 1/6$. Top panel: Illustration of the symplectic local pairing symmetry, Eq. (13), for the Gram-Schmidt exponents ${}^{(+)}\Lambda_2^{GS}$ and ${}^{(+)}\Lambda_3^{GS}$ (smooth red lines). Here, $D = 4$. Also the inequality Eq. (15) applies ($\ell = 2$), as the dashed green line for ${}^{(-)}\Lambda_3^{GS}$ certifies. Bottom panel: Verification of the time-reversal invariance property (16) for the covariant vectors specified.

VII. CONCLUDING REMARKS

For the doubly-thermostated oscillator in a nonequilibrium stationary state, there is a single vanishing global exponent, λ_2, due to the time-translation invariance of the equations of motion. The corresponding covariant vector, $\boldsymbol{v}^2(t)$, needs to be parallel (or antiparallel) to the phase-space velocity $\dot{\boldsymbol{\Gamma}}(t) \equiv \{\dot{q}(t), \dot{p}(t), \dot{z}(t), \dot{x}(t)\}$. We have verified in our simulation that this is indeed the case. The remaining vectors $\boldsymbol{v}^1$, $\boldsymbol{v}^3$ and $\boldsymbol{v}^4$ are oriented with angles fluctuating between 0 and π with respect to $\dot{\boldsymbol{\Gamma}}(t)$. The Gram-Schmidt vectors behave very differently. Whereas the vector $\boldsymbol{g}^1$ is identical to $\boldsymbol{v}^1$, the vector $\boldsymbol{g}^2$ is not parallel to $\dot{\boldsymbol{\Gamma}}(t)$. Instead, the vectors $\boldsymbol{g}^3$ and $\boldsymbol{g}^4$

are perpendicular to $\dot{\boldsymbol{\Gamma}}(t)$ as expected in view of the covariant subspaces of Eq. (10). These observations serve as convenient consistency checks for the numerical procedure.

One of the remarkable features of the covariant local Lyapunov exponents $\Lambda^{cov}(\boldsymbol{\Gamma}(t))$ is their singular behavior transverse to the phase flow, whereas they are absolutely continuous in the direction of the flow. Fig. 9 provides an illuminating example. The singularities are consequences of bifurcations in the past history. Still, the local exponents are point functions in the phase space in the sense that one always gets the same value at the state point in question, as long as the trajectory has been followed from far enough back and has experienced the same history. Due to the uniqueness of the solutions of differential equations there is only this path to the state point in question. The global exponents, however, are time averages of the local exponents along an (ergodic) trajectory.

A final remark concerns the doubly-thermostated driven oscillator again. In a driven system (in our case a single particle in a non-homogenous thermal field) heat and, hence, entropy is generated, which needs to be compensated by a negative entropy production in the thermostat to achieve a stationary state. The excess heat is transferred from the system to the thermostat (by the positive friction $zp > 0$), where it disappears. It follows from the thermostated motion equations in Sec. V A that the external entropy production (of the reservoir) is given by

$$\dot{S}/k \equiv \frac{\partial}{\partial \boldsymbol{\Gamma}} \cdot \dot{\boldsymbol{\Gamma}} = z + x,$$

where k is the Boltzmann constant. In the nonequilibrium situation, a full time average $\langle z + x \rangle$ is necessarily positive. However, we have verified by simulation that finite time averages of this quantity numerically obey the steady-state fluctuation theorem originally discovered by Evans, Cohen and Morriss [32]. This theorem was given a firm theoretical basis by Gallavotti and Cohen [33, 34], by invoking the so-called 'chaotic hypothesis' for Anosov-like systems. Although our system is not Anosov-like, it still obeys the theorem.

VIII. ACKNOWLEDGEMENTS

[1] B.L. Holian, Wm. G. Hoover, and H.A. Posch, Phys. Rev. Lett. **59**, 10 (1987).

[2] Wm. G. Hoover, *Time reversibility, computer simulation,*

and chaos, World Scientific, Singapore, 1999.

[3] H. A. Posch and Wm. G. Hoover, Journal of Physics: Conference Series **31**, 9, (2006).

[4] V.I. Oseledec, Trudy Moskov. Mat. Obsc. **19**, 179, (1968). English transl. Trans. Moscow Math. Soc. **19**, 197 (1968).

[5] D. Ruelle, Publications Mathématiques de l'IHÉS **50**, 27 (1979).

[6] J.-P. Eckmann and D. Ruelle, Rev. Mod. Phys. **57**, 617 (1985).

[7] H. Bosetti and H.A. Posch, Chem. Phys. (2010), doi:10.1016/j.chemphys.2010.06.010

[8] G. Benettin, L. Galgani, A. Giorgilli, and J.-M. Strelcyn, Meccanica **15**, 21 (1980).

[9] I. Shimada and T. Nagashima, Prog. Theor. Phys. **61**, 1605 (1979).

[10] A. Wolf, j.B. Swift, H.L. Swinney, and J.A. Vastano, Physica D **16**, 285 (1985).

[11] W.H. Press, S.A. Teukolsky, W.T. Vetterling, and B.P. Flannery, *Numerical Recipes in Fortran 77: The Art of Scientific Computing*, Cambridge University Press, Cambridge, 1999.

[12] F. Ginelli, P. Poggi, A. Turchi, H. Chaté, R. Livi, and A. Politi, Phys. Rev. Lett. **99**, 130601 (2007).

[13] I. Goldhirsch, P.-L. Sulem, and S.A. Orszag, Physica D **27**, 311 (1987).

[14] H.A. Posch and Wm. G. Hoover, Phys. Rev. A **38**, 473 (1988).

[15] H. A. Posch and Wm. G. Hoover, Physica D **187**, 281 (2004).

[16] H.A. Posch, C. Dellago, Wm.G. Hoover, and O. Kum, in *Pioneering Ideas for the Physical and Chemical Sciences: Josef Loschmidt's Contributions and Modern Developments in Structural Organic Chemistry, Atomistics, and Statistical Mechanics*, W. Fleischhacker and T. Schönfeld, eds., Plenum, New York, 1997; p. 233.

[17] H.-D. Mayer, J. Chem. Phys. **84**, 3147 (1986).

[18] G.J. Martyna, M.L. Klein, and M. Tuckerman, J. Chem. Phys. **97**, 2635 (1992).

[19] Wm.G. Hoover, C.G. Hoover, and H.A. Posch, Comp. Meth. in Science and Technology **7**, 55 (2001).

[20] Wm.G. Hoover, H.A. Posch, and C.G. Hoover, J. Chem. Phys. **115**, 5744 (2001).

[21] J.-P. Eckmann, Ch. Forster, H.A. Posch, and E. Zabey, J. Stat. Phys. **118**, 813 (2005).

[22] Y.A. Kuznetsov, *Elements of Applied Bifurcation Theory*, Applied Mathematical Sciences Vol. 112, Springer, NewYork, 2004.

[23] Hadrien Bosetti, thesis (University of Vienna, 2010).

[24] P. Gaspard, Phys. Rev. E **53**, 4379 (1996).

[25] P. Gaspard, *Chaos, Scattering and Statistical Mechanics*, Cambridge University Press, Cambridge, 1998, p. 308.

[26] C. Dellago and Wm. G. Hoover, Physics Lett. A **268**, 220 (2000).

[27] Wm.G. Hoover, C.G. Hoover, and H.A. Posch, Phys. Rev. A **41**, 2999 (1990).

[28] Wm.G. Hoover, C.G. Hoover, and F. Grond, Comp. Meth. in Science and Technology **13**, 1180 (2008).

[29] M. Hénon, Comm. Mathem. Phys. **50**, 69 (1976).

[30] A.J. Lichtenberg and M.A. Lieberman, *Regular and Stochastic Motion*, Springer, New York, 1983.

[31] R. Ramaswamy, Eur. Phys. J. B **29**, 339 (2002).

[32] D.J. Evans, E.G.D. Cohen, and G.P. Morriss, Phys. Rev. Lett. **71**, 2401 (1993).

[33] G. Gallavotti and E.G.D. Cohen, Phys. Rev. Lett. **74**, 2694 (1995).

[34] G. Gallavotti and E.G.D. Cohen, J. Stat. Physics **80**, 931 (1995).